International Conference on Radar Systems (RADAR 2022), 24-27 October 2022, Edinburgh, UK
https://ieeexplore.ieee.org/document/10038898

Laboratory Multistatic Polarimetric 3D SAR

Daniel Andre[1*], Richard Welsh[1], Mark Finnis[2]

[1] Centre for Electronic Warfare, Information and Cyber, Cranfield University, Defence Academy of the United Kingdom, Shrivenham, UK.
[2] Centre for Defence Engineering, Cranfield University, Defence Academy of the United Kingdom, Shrivenham, UK.
**Daniel.Andre@cranfield.ac.uk*

Keywords: SAR, BISATIC, MULTISTATIC, VOLUMETRIC, 3D, POLARIZATION

Abstract

With the advent of constellations of SAR satellites, and the possibility of swarms of SAR UAV's, there is increased interest in multistatic SAR image formation. This may provide advantages including allowing three-dimensional image formation free of clutter overlay; the coherent combination of bistatic SAR geometries for improved image resolution; the collection of additional scattering information, including polarimetric. The polarimetric collection may provide useful target information, such as its orientation, polarizability or number of interactions with the radar signal; distributed receivers would be more likely to capture any bright specular responses from targets in the scene, making target outlines distinct. Highlight results from multistatic polarimetric SAR experiments at the Cranfield University GBSAR laboratory are presented, illustrating the utility of the approach.

1. Introduction

With the advent of constellations of Synthetic Aperture Radar (SAR) satellites, and the possibility of swarms of SAR Unmanned Aerial Vehicles (UAV)'s [1], there is increased interest in multistatic SAR image formation.

These types of collections may provide advantages including allowing three-dimensional (3D) image formation free of clutter overlay; the coherent combination of bistatic SAR geometries for improved image resolution; the collection of additional scattering information, including polarimetric.

Polarimetric collection may provide useful target information, such as scatterer orientation, polarizability or number of interactions with the radar signal [2,3,5]; distributed receivers would be more likely to capture any bright specular responses from targets in the scene, making target outlines distinct.

Highlight results from multi-static polarimetric SAR experiments at the Cranfield University GBSAR laboratory [4] are presented, illustrating the utility of the approach.

2. Bistatic polarimetric decomposition

Whilst monostatic polarimetric decompositions are well understood, bistatic generalizations of these are not well-known and the physical interpretation of many proposed are not clear. Some bistatic decomposition approaches are only slight modifications of existing monostatic approaches, for example simply introducing an anti-symmetric component to the target scattering matrix (which is always symmetric in the monostatic case). However the physical meaning associated with this polarimetric parameter extraction may be unclear, and increasingly so where the geometry is far from the mono-static case.

The approach selected for application in this work, is that described by Titin-Schnaider [2,3,5] constituting a bistatic generalization of the Huynen Fork parameter decomposition [8], providing six polarimetric parameters: for the bi-static case there are two Orientation angles and two Symmetry angles associated with the incident and scattered ray directions. The formalism has been related to a generalization of the Cloude-Pottier parameters [5].

The bistatic generalization of the Huynen Fork target parameters was found to provide a physically meaningful pixel based polarimetric decomposition [2]. In the mono-static case there are four parameters of interest θ τ ν γ (theta, tau, nu, gamma) representing:

- **Orientation / Tilt angle**, θ: linked to the angle between the projection of the scatterer main axis and the horizontal reference angle: $-90° \leq \theta \leq 90°$. Here we define a positive rotation as clockwise about the down-range direction. Scatterers for which the tilt angle may be meaningful include rods / dipoles and straight edges of extended objects.

- **Symmetry angle**, τ: allowing the separation of symmetric and non-symmetric scatterers. A symmetric scatterer is symmetric about a plane containing the incident ray, $0° \leq |\tau| \leq 45°$, where 0° indicates high symmetry, and $|\tau| = 45°$ indicates low symmetry. Scatterers with high symmetry would include spheres, rods / dipoles and corner reflectors.

- **Skip angle**, ν: divides scatters into two classes according, approximately, to whether the scattered rays have had an odd or even number of bounces: $0° \leq |\nu| \leq 45°$, where 0° indicates an Odd-bounce interaction and $|\nu|=45°$ indicates an Even-bounce interaction. Odd-bounce scatterers include spheres, flat plates and trihedral multi-bounce. Even-bounce scatterers include dihedral multi-bounce. Note that at certain aspects the dihedral response may be dominated by single flat plate responses or straight edge diffraction.
- **Polarizability angle**, γ: in this approach is taken to mean that the scatterer only returns waves with a particular polarization regardless of incident polarization, hence a polarization projection: $0° \leq \gamma \leq 45°$, where 0° indicates high polarizability and 45° low. Scatterers with medium to high polarizability include rods and the straight edges of extended objects. Scatterers with low polarizability include spheres, flat plates, and corner reflectors with multi-bounce including both dihedrals and trihedrals.

For the bistatic case there are two τ parameters, τi τs, and two θ parameters, θi θs, where "i" stands for the incident direction, and "s" for the scattered direction. In the monostatic case these directions are equivalent, so that the τ values become the same, and the θ values become the same. It is noted that once the orientation parameters are determined (θi, θs), the additional Huynen parameters provide information intrinsic to the electro-magnetic mechanism itself, that is, independent of input and output antenna orientations.

2.1. Laboratory measurements

The GBSAR laboratory performs microwave measurements with a Vector Network Analyser (VNA), which generates a stepped frequency waveform. The system is currently set up for indoor use, with the VNA attached to two Ultra-Wideband horn antennas allowing measurements within the range 1-10 GHz. The Antennae can be mounted in a bistatic or a pseudo monostatic configuration.

When in a bistatic configuration, seen in Fig. 1, each antenna is mounted on a different two-dimensional vertical SAR aperture scanner. One SAR aperture is 3.5 m wide by 1.5 m high, this one used for the transmitter, and the other is 1.3 m wide by 1.5 m high, used for the receiver, as seen in Figure 1.

When a SAR scene is left undisturbed, and transmitter trajectories are precisely repeated, the combination of repeat scans with the receiver in different locations (or trajectories) will be equivalent to a multistatic scan with multiple receivers operating simultaneously. Using this approach, multistatic scans have been collected in the GBSAR lab, even though the VNA has only two ports.

Fig. 1. The GBSAR laboratory in a bistatic configuration.

The multistatic geometry chosen for this collection is shown in Fig. 2. The transmitter traverses the vertical rectangular aperture in blue, with Nyquist positional sampling, and nine fixed receiver positions utilised for nine bistatic 3D SAR collections are to the left of the scene, numbered in the figure.

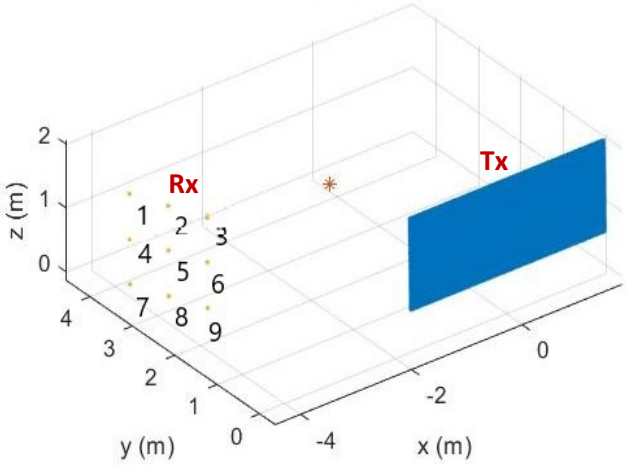

Fig. 2 Multistatic 3D SAR geometry, with 2D SAR aperture transmitter trajectory in blue, and nine fixed receiver positions to the left of the scene.

The measured target scene for the results presented here consisted of a quarter scale T72 tank model placed on gravel and reference spheres, seen in Fig. 3. The gravel provides a speckle background, with shadowing visible, depending on SAR geometry.

Fig. 3 Target scene, consisting of a Quarter scale T72 tank model on gravel, and reference sphere "S".

3. Results

3.1. Multistatic data summation

A multistatic polarimetric laboratory collection was performed, providing thirty-six bistatic 2D SAR aperture scans: nine bistatic scans, for each of four linear polarization channels. With this data, thirty-six 3D volumetric bistatic SAR image results were generated with the bistatic Backprojection SAR image formation algorithm (BPA).

An incoherent sum of the nine bistatic 3D SAR image VV polarization results, provided initial volumetric images for inspection, corresponding maximum-intensity projections (MIPs) are presented in Fig. 4, with the down-range direction up the page. The 3D structure of the target and scene is evident. The shadowing to the rear of the model is not discernible, due to the wide transmitter SAR aperture, however the shadow to the right of the vehicle, associated with the static receiver directions, is evident. The large sphere to the rear-right of the scene is marked "S", and several associated multipath features are visible, one directly at ground level below the sphere, and the other symmetrically below ground level.

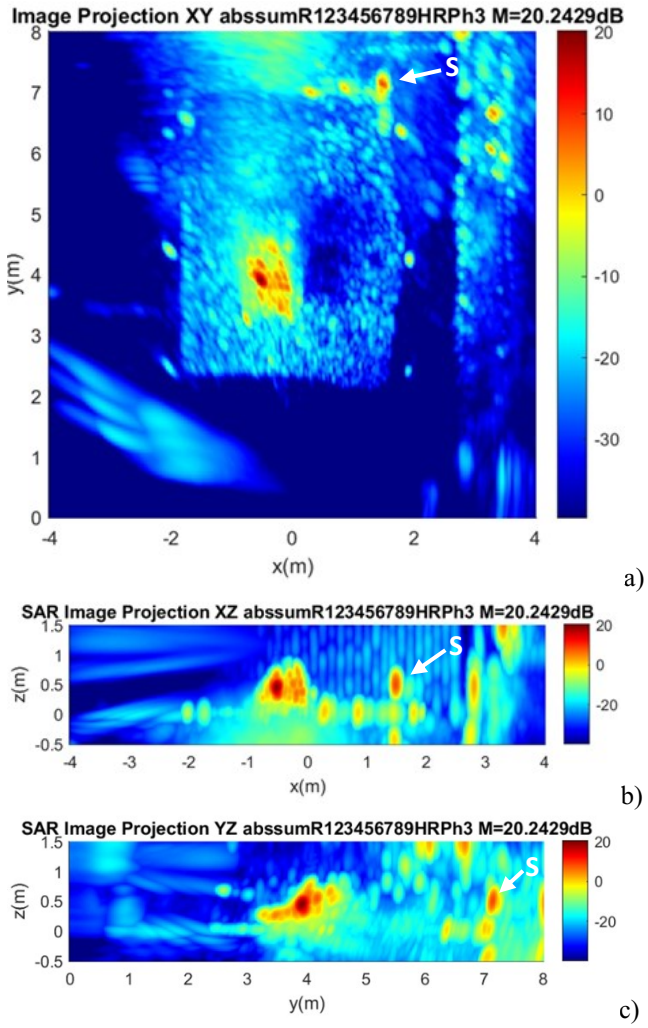

Fig. 4 MIPs of an incoherent sum of the nine VV polarization 3D bistatic SAR images, with a z-projection (a), y-projection (b) and an x-projection (c). The large reference sphere is marked "S".

Having evaluated the incoherent sum result, a coherent sum of the nine bistatic 3D SAR image VV polarization results was performed. Coherent sums are however very sensitive to positional errors in SAR geometry information. It is estimated that a 4 mm range error in antenna ground truth, could give rise to as much as 90° of phase error at 10 GHz. Such a recorded error size would be possible in the ground-truth taking process, in directions perpendicular to the linear scanner actuators. (However, in the directions of the linear scanner actuators the accumulated positional errors after many thousands of moves were confirmed to be lower than 0.1 mm). Indeed, after forming an initial coherent sum, the result was seen to be defocussed.

A data-driven phase correction algorithm was developed, maximizing the intensity of the brightest scene scatterer in any given VV image pair coherent sum, providing an overall phase correction value for each of the nine bistatic SAR geometries. The result of the phase corrected nine VV polarization image coherent sum is presented in Fig. 5, in the form of MIPs.

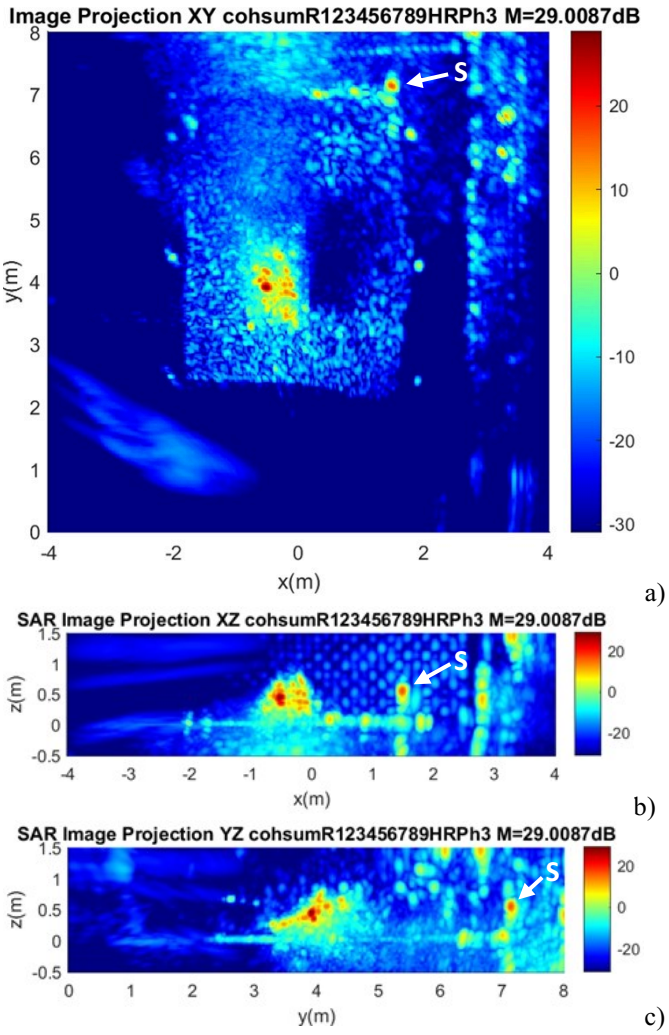

Fig 5. MIPs of a phase corrected coherent sum of the nine VV polarization 3D bistatic SAR images, with a z-projections (a), y-projection (b) and an x-projection (c). The large reference sphere is marked "S".

An increase in SAR resolution in all three spatial dimensions has resulted from the phase corrected coherent summation, over the incoherent summation, providing finer detail across the main target and scene.

3.2. Polarimetric decomposition of scene

The bistatic generalized Huynen decomposition has undergone previous evaluation with canonical scatterers, both in the literature [3] and in the GBSAR laboratory. In the current study, results for the complex scene, are presented. The decomposition was applied to both the individual bistatic polarimetric images, and to the image sums. Volumetric SAR MIPs are presented for the phase corrected multistatic summed bistatic polarimetric images in Fig. 6 and 7, with the pertaining colour maps shown in Fig. 8, and selected features marked in the first and last images of the polarimetric set.

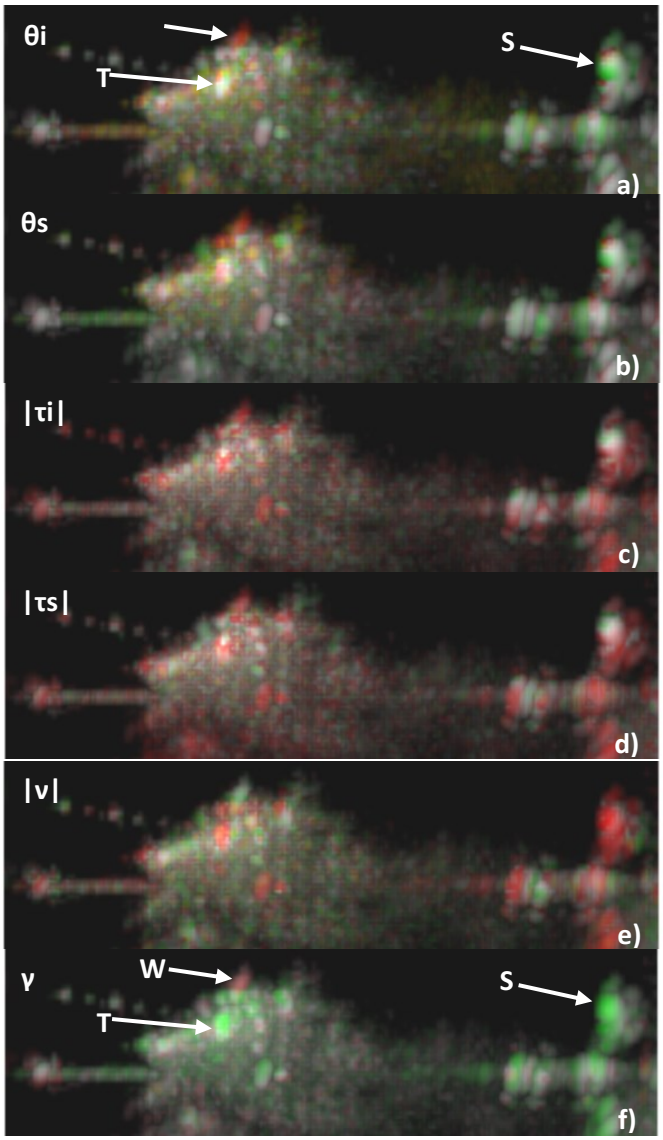

Fig. 6. Side-view Polarimetric decomposed MIPs showing θi, θs, |τi|, |τs|, |ν|, γ in a) to f) respectively, with colour maps presented in Fig. 8.

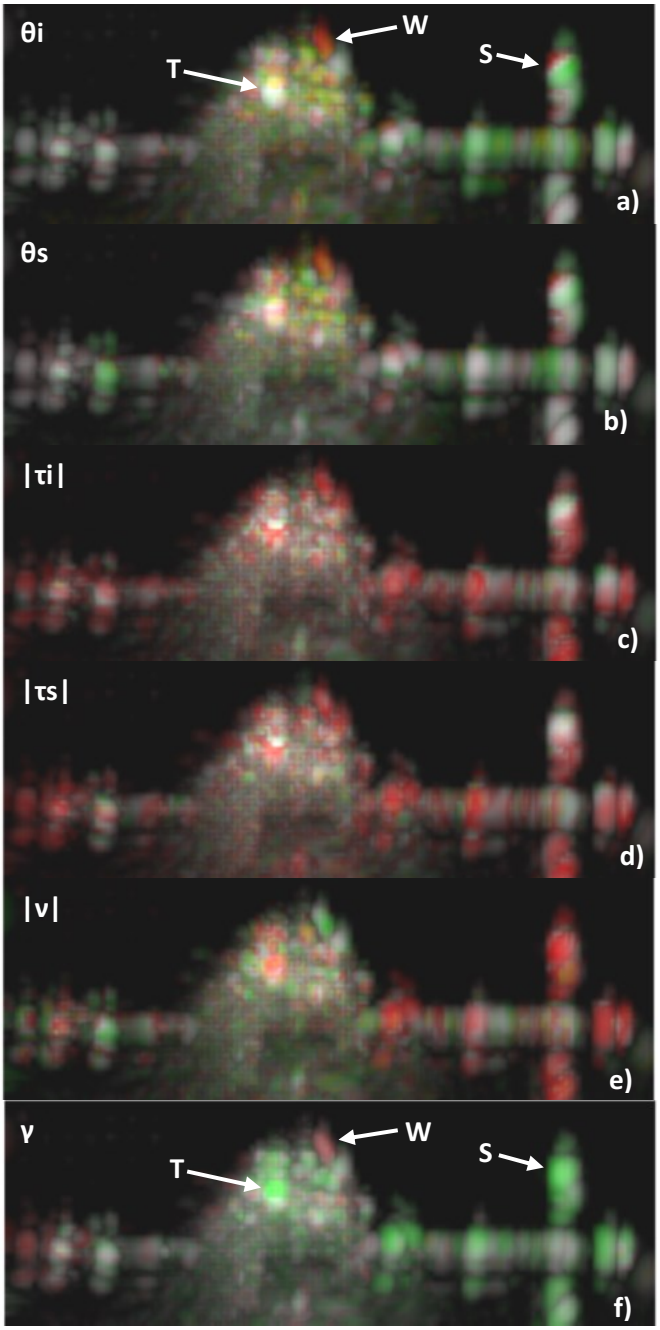

Fig. 7. Front-view polarimetric decomposed MIPs showing θi, θs, |τi|, |τs|, |ν|, γ in a) to f) respectively, with colour maps presented in Fig. 8.

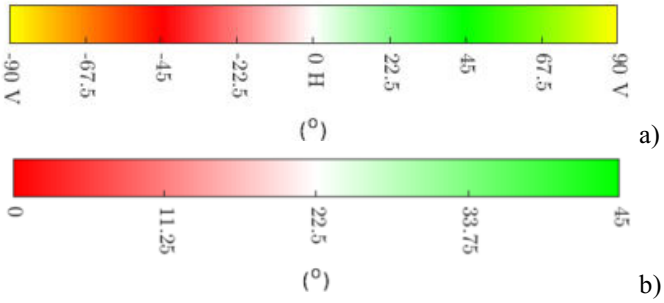

Fig. 8. Colour maps associated with Bistatic Huynen decomposition parameters θi, θs (a) and |τi|, |τs|, |ν|, γ (b).

Note that for the SAR geometries investigated (seen in Figure 2), it was found that scatterers retained their polarimetric properties, both across the nine bistatic SAR geometries and in the phase corrected coherent sum. Only results from the coherent sum are presented here.

Firstly, the large reference sphere "S", is behaving mostly as expected, with: low polarizability γ (green); Odd-bounce |ν| (red); an unstable and meaningless set of orientations θi, θs as expected; the symmetry |τi|, |τs| values seem unstable however.

The T72 scale model shows a complex variety of scattering behaviour across it, and it is difficult to ascertain the origin of many features in MIP results alone, however some features are highlighted here.

The antenna wire on the model, marked "W" in the photographs in Fig. 9, and in the MIPS in Fig. 6-7, was tied down to the model body, and is consequently in the form of an arc. Parts of this component would be expected to behave as a dipole scatterer. This scatterer is behaving mostly as expected, with: high polarizability γ (red); orientations θi, θs in the region of ~67° (red-orange); high symmetry |τi|, |τs| (red); however it is Even-bounce |ν| (green).

A region on the side of the model T72 turret, marked "T" in Fig. 9b), gives rise to a strong and stable specular scattering result in the bistatic SAR geometries. This concave surface specular scatterer is behaving as expected, with: low polarizability γ (green); Odd-bounce |ν| (red); high symmetry |τi|, |τs| (red); unstable and meaningless orientations θi, θs as expected.

Fig. 9. Close-up side-views of the quarter scale T72 tank model. The highlighted parts are the arched antenna wire "W", and the bistatic specular reflection point on the turret "T".

Other scatterers may be seen more clearly by rotating and slicing the polarimetric volumetric renderings within viewing software. The analysis of the results is ongoing and involves determining additional polarimetric data visualization techniques.

4. Conclusion

Multistatic polarimetric SAR measurements of a complex target and scene were conducted at the GBSAR laboratory, to determine benefits of these type of collection geometries.

Results have been presented which combine multiple bistatic SAR collections to provide 3D SAR (volumetric) images of the scene. Incoherent summation of the individual bistatic collections provides a useful result, allowing a clear determination of the target, however with the SAR geometries utilized, a phase corrected coherent summation of the nine bistatic SAR collections was shown to provide results with a much-improved SAR resolution in all three spatial dimensions.

A bistatic generalized Huynen decomposition was applied to the data, and for the SAR geometries investigated, it was found that scatterers retained their polarimetric properties, both across the nine bistatic SAR geometries and in the phase corrected coherent sum.

Maximum intensity projections were presented, and specific scatterers were highlighted, along with their scattering characteristics. The analysis of the results is ongoing, and involves determining additional polarimetric data visualization techniques.

5. Acknowledgements

This work was sponsored by the Defence Science and Technology Laboratory (DSTL).

6. References

1. A. Horne, A. Blake, A. L. Qinetiq, C. Stevenson, M. Nottingham, D. Muff, D. Blacknell, "Exploration of Multidimensional Radio Frequency Imaging to Derive Remote Intelligence of Building Interiors", in 2018 international Conference on Radar, RADAR 2018, Institute of Electrical and Electronics Engineers Inc., Dec 2018
2. Titin-Schnaider, C. "Polarimetric Characterization of Bistatic Coherent Mechanisms", IEEE Transactions on Geoscience and Remote Sensing, Vol.46, No.5, May 2008
3. Titin-Schnaider, C., "Physical Meaning of Bistatic Polarimetric Parameters", IEEE Transactions on Geoscience and Remote Sensing, Vol.48, No.5, May 2010
4. Corbett, B., Andre, D., Finnis, M.: 'Localising vibrating scatterer phenomena in synthetic aperture

radar imagery', Electron. Lett., 2020, 56, pp. 395-398
5. Titin-Schnaider, C., "Characterization and Recognition of Bistatic Polarimetric Mechanisms", IEEE Transactions on Geoscience and Remote Sensing, Vol.51, No.3, March 2013
6. D. Andre, K. Morrison, D. Blacknell, D. Muff, M. Nottingham, and C. Stevenson, "Very High Resolution Coherent Change Detection," 2015.
7. D. Andre, D. Blacknell, and K. Morrison, "Spatially variant incoherence trimming for improved SAR CCD," 2013.
8. Huynen, J. R., "Phenomenological Theory of Radar Targets", PhD Thesis, TU Delft, 1970
9. Sarabandi, K., Ulaby, F., Tassoudji, M., "Calibration of Polarimetric Radar Systems with Good Polarization Isolation", IEEE Transactions on Geoscience and Remote Sensing, Vol.28, No.1, January 1990